J|A|C|S
ARTICLES
Published on Web 05/05/2006

Compositional Dependence of Negative Thermal Expansion in the Prussian Blue Analogues $M^{II}Pt^{IV}(CN)_6$ (M = Mn, Fe, Co, Ni, Cu, Zn, Cd)

Karena W. Chapman,[†,§] Peter J. Chupas,[‡] and Cameron J. Kepert*[,†]

Contribution from the School of Chemistry, University of Sydney, Sydney, NSW 2006, Australia, and Advanced Photon Source, Argonne National Laboratory, Argonne, Illinois 60439

Received February 14, 2006; E-mail: c.kepert@chem.usyd.edu.au

Abstract: The effect of M^{II} substitution on the magnitude of the negative thermal expansion (NTE) behavior within a series of Prussian Blue analogues, $M^{II}Pt^{IV}(CN)_6$ for M^{II} = Mn, Fe, Co, Ni, Cu, Zn, Cd, has been investigated using variable-temperature powder X-ray diffraction (100−400 K). The NTE behavior varies widely with M^{II} substitution, from near zero thermal expansion in $NiPt(CN)_6$ ($\alpha = dl/l\,dT = -1.02(11) \times 10^{-6}\ K^{-1}$) up to a maximum in $CdPt(CN)_6$ ($\alpha = -10.02(11) \times 10^{-6}\ K^{-1}$). The trend in the magnitude of the NTE behavior, with increasing atomic number (Z) of the M^{II} ion, follows the order $Mn^{II} > Fe^{II} > Co^{II} > Ni^{II} < Cu^{II} < Zn^{II} < Cd^{II}$, which correlates with the trends for M^{II} cation size, the lattice parameter, and structural flexibility as indicated by the temperature-dependent structural refinements and Raman spectroscopy. Analysis of the temperature dependence of the average structures suggests that the differences in the thermal expansion are due principally to the different strengths of the metal−cyanide binding interaction and, accordingly, the different energies of transverse vibration of the cyanide bridge, with enhanced NTE behavior for more flexible lattices.

Introduction

While the vast majority of materials increase in dimension upon heating, the opposite behavior has been recognized in certain materials. Such negative thermal expansion (NTE) materials are not only of fundamental interest but have important potential applications, most notably in compensating for the more common positive thermal expansion (PTE) behavior of other materials.[1−4] Pivotal to the development and design of materials with enhanced NTE behavior or with thermal expansivities optimized toward specific applications is the understanding of the role of the chemical composition and structure, particularly as related to the magnitude of the observed NTE effect or the coefficient of thermal expansion (CTE, $\alpha = dl/ldT$).

Perhaps the most widely studied type of NTE material includes a range of oxides formed by strong single-atom bridges such as in the AM_2O_8,[5−8] AM_2O_7,[9,10] $A_2M_3O_{12}$,[11] zeolite,[12−14] and ReO_3[15] families. The origin of NTE behavior in these materials has been widely studied: the thermal population of low-energy transverse vibrational modes of the bridging atoms, with relatively minor expansion of individual bonds, draws the strongly bridged metal centers closer together, giving rise to the observed contraction of the lattice parameter.[8,16,17] However, it has been difficult to systematically probe the influence of structure and composition, such as by chemical substitution, on the extent of the NTE effect in such oxides.[9,11,12,18,19] This is due, in part, to the rich structural chemistry of the inorganic oxides, which is often associated with slightly different structural motifs, superstructures, subtle ordering effects, phase transitions, and, accordingly, complex (nonlinear and anisotropic) thermal expansion behavior.

Recently, NTE behavior has been identified in a number of cyanide-based molecular framework materials including in the $M(CN)_2$[17,20,21] and Prussian Blue[22,23] families. The NTE behavior of these expanded frameworks originates from a transverse

† University of Sydney.
‡ Argonne National Laboratory.
§ Present address: Argonne National Laboratory, Argonne, IL 60439.

(1) Roy, R.; Agrawal, D. K.; McKinstry, H. A. *Annu. Rev. Mater. Sci.* **1989**, *19*, 59−81.
(2) Sleight, A. W. *Annu. Rev. Mater. Sci.* **1998**, *28*, 29−43.
(3) Evans, J. S. O. *J. Chem. Soc., Dalton Trans.* **1999**, 3317−3326.
(4) Barrera, G. D.; Bruno, J. A. O.; Barron, T. H. K.; Allan, N. L. *J. Phys.: Condens. Matter* **2005**, *17*, R217−R252.
(5) Martinek, C.; Hummel, F. A. *J. Am. Ceram. Soc.* **1968**, *51*, 227−228.
(6) Mary, T. A.; Evans, J. S. O.; Sleight, T. V. A. W. *Science* **1996**, *272*, 90−92.
(7) Lind, C.; Wilkinson, A. P.; Hu, Z. B.; Short, S.; Jorgensen, J. D. *Chem. Mater.* **1998**, *10*, 2335−2337.
(8) Evans, J. S. O.; David, W. I. F.; Sleight, A. W. *Acta Crystallogr., Sect. B* **1999**, *55*, 333−340.
(9) Taylor, D. *Br. Ceram. Trans. J.* **1988**, *87*, 39−45.
(10) Korthuis, V.; Khosrovani, N.; Sleight, A. W.; Roberts, N.; Dupree, R.; Warren, W. W. *Chem. Mater.* **1995**, *7*, 412−417.
(11) Evans, J. S. O.; Mary, T. A.; Sleight, A. W. *J. Solid State Chem.* **1997**, *133*, 580−583.
(12) Lightfoot, P.; Woodcock, D. A.; Maple, M. J.; Villaescusa, L. A.; Wright, P. A. *J. Mater. Chem.* **2001**, *11*, 212−216.
(13) Woodcock, D. A.; Lightfoot, P.; Villaescusa, L. A.; Diaz-Cabanas, M. J.; Camblor, M. A.; Engberg, D. *Chem. Mater.* **1999**, *11*, 2508−2514.
(14) Attfield, M. P.; Sleight, A. W. *Chem. Mater.* **1998**, *10*, 2013−2019.
(15) Tao, J. Z.; Sleight, A. W. *J. Solid State Chem.* **2003**, *173*, 45−48.
(16) Tao, J. Z.; Sleight, A. W. *J. Solid State Chem.* **2003**, *173*, 442−448.
(17) Chapman, K. W.; Chupas, P. J.; Kepert, C. J. *J. Am. Chem. Soc.* **2005**, *127*, 15630−15636.
(18) Evans, J. S. O.; Hanson, P. A.; Ibberson, R. M.; Duan, N.; Kameswari, U.; Sleight, A. W. *J. Am. Chem. Soc.* **2000**, *122*, 8694−8699.
(19) Li, J.; Sleight, A. W.; Jones, C. Y.; Toby, B. H. *J. Solid State Chem.* **2005**, *178*, 285−294.

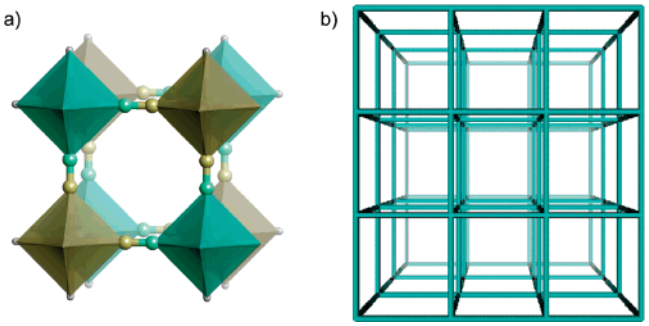

Figure 1. Illustrations of the structure of the Prussian Blue family indicating (a) the $M^{II}N_6$ (green) and $Pt^{IV}C_6$ (yellow) octahedra and (b) the cubic (expanded ReO_3 or α-Po) network topology.

vibrational mechanism analogous to that of the oxides; however, the additional dynamic flexibility associated with the double-atom (M−CN−M′) rather than single-atom (e.g., M−O−M′) bridges gives rise to an increased number of low-energy lattice vibrations that can contribute to the NTE behavior. Hence, there exists a greater capacity for NTE in cyanide-based systems. To highlight this point, considerably more negative CTEs have been reported for cyanide-bridged Prussian Blue analogues,[22,23] which have an expanded ReO_3 topology, as compared to the ReO_3-type TaO_2F, which has extremely low thermal expansion.[15] In this case, the NTE contribution from the transverse vibrational motion counterbalances the PTE contribution from the expansion of the individual Ta−O and Ta−F bonds, resulting in close to zero thermal expansion behavior.

One of the features of molecular framework materials that largely underlies the present rapid development of the area is the enhanced level of structural control and flexibility that may be achieved through crystal engineering.[24,25] This opens the possibility of systematically varying the compositional and topological structure of cyanide-based molecular framework materials to investigate the factors that influence NTE behavior. This is particularly true within the Prussian Blue family, for which a large number of phases are known.[26,27] The Prussian Blue analogues form with various combinations of octahedral metal ions, and, as such, this family provides an attractive system in which to study the influence of metal ion substitution on NTE behavior within an isostructural series.

Of the many known Prussian Blue analogues, the $M^{II}Pt^{IV}(CN)_6$ series is ideally suited a comparative investigation of NTE behavior, with the linear bridging of alternating $Pt^{IV}C_6$ and $M^{II}N_6$ octahedra forming a cubic network[28,29] without the lattice vacancies and cationic guests found in some Prussian Blue phases (Figure 1).[30,31] As such, noncoordinated guest water molecules contained within the pores of the as-synthesized framework can be removed at elevated temperatures while retaining the framework structure,[23] allowing a direct comparison of the thermal expansion behavior intrinsic to each lattice.

Here, we explore the effect of the systematic variation of the divalent metal ion (M^{II}) site on the NTE behavior in the series of Prussian Blue analogues $M^{II}Pt^{IV}(CN)_6$ for M = Mn, Fe, Co, Ni, Cu, Zn, Cd, using variable-temperature powder X-ray diffraction (100−400 K). Our analyses of the Rietveld refined structures show a correlation of the magnitude of the NTE behavior with cation size, lattice parameter, and structural flexibility, as well as the lattice vibrational energies as determined by Raman spectroscopy. The results suggest that the magnitude of the NTE behavior is largely influenced by the vibrational flexibility of the metal−cyanide binding interaction, with enhanced NTE behavior for more flexible frameworks.

Experimental Methods

Sample Preparation. Crystalline samples of the hydrated Prussian Blue analogues, $M^{II}Pt^{IV}(CN)_6{\cdot}2\{H_2O\}$, containing noncoordinated guest water molecules were prepared by slow diffusion of aqueous solutions of the nitrate or chloride metal(II) salts and $K_2Pt^{IV}(CN)_6$. A solution of $K_2Pt^{IV}(CN)_6$ (Aldrich, 3 mL, 0.17 M) was carefully layered above a solution of $M^{II}(NO_3)_2{\cdot}x\{H_2O\}$ or $M^{II}Cl_2{\cdot}x\{H_2O\}$ (0.5 mL, 1.0 M) in a small glass vial. The very pale green (M = Mn), pale yellow (Fe), pale pink (Co), pale blue (Ni), pale green-blue (Cu), and colorless (Zn, Cd) crystalline products formed within 1−2 weeks and were filtered, washed with water and ethanol, and dried in air.

Powder X-ray Diffraction. Polyimide capillary loaded samples of $M^{II}Pt^{IV}(CN)_6{\cdot}2\{H_2O\}$ (M = Mn, Fe, Co, Ni, Cu, Zn, Cd) were dehydrated in situ at 433 K under continuous helium (UHP) flow using an apparatus that allows simultaneous heating and gas flow.[32] The dehydrated samples, $M^{II}Pt^{IV}(CN)_6$, were cooled to a nominal temperature of 85 K using an Oxford Cryosystems Cryostream 700. Data were collected in 3 min exposures with continuous heating at a rate of 100 K h^{-1} to a maximum temperature of 400 K under a helium atmosphere. This corresponds to the collection of diffraction images at 7 K intervals. A temperature correction (see Supporting Information) was applied to the nominal temperature of the cryostream obtained from a calibration run using the same experimental setup with an Omega K-type thermocouple added at the sample position such that the actual temperature range of the experiment was ca. 100−400 K. The X-rays (90.48 keV, $\lambda = 0.13702$ Å) available at the 11-ID-B beamline at the Advanced Photon Source at Argonne National Laboratory[33,34] were used in combination with a MAR-345 imaging plate (IP) detector to record diffraction patterns.[35] The raw images were processed using Fit-2D.[36,37] The sample-to-detector distance and tilt of the IP relative to the beam were refined using a LaB_6 standard.

Rietveld analyses of the variable-temperature diffraction data were performed within GSAS.[38] Details of the Rietveld refinements are included in the Supporting Information. The linear CTEs were estimated by a least-squares straight line fit to the data. Values of the lattice parameter, lattice volume, and structural parameters referenced to particular temperatures were calculated from a least-squares linear fit

(20) Williams, D. J.; Partin, D. E.; Lincoln, F. J.; Kouvetakis, J.; O'Keeffe, M. *J. Solid State Chem.* **1997**, *134*, 164−169.
(21) Goodwin, A. L.; Kepert, C. J. *Phys. Rev. B* **2005**, *71*, 140301(R).
(22) Margadonna, S.; Prassides, K.; Fitch, A. N. *J. Am. Chem. Soc.* **2004**, *126*, 15390−15391.
(23) Goodwin, A. L.; Chapman, K. W.; Kepert, C. J. *J. Am. Chem. Soc.* **2005**, *127*, 17980−17981.
(24) Hoskins, B. F.; Robson, R. *J. Am. Chem. Soc.* **1990**, *112*, 1546−1554.
(25) Robson, R. *J. Chem. Soc., Dalton Trans.* **2000**, 3735−3744.
(26) Dunbar, K. R.; Heintz, R. A. *Prog. Inorg. Chem.* **1997**, *45*, 283−391.
(27) Ritter, S. K. *Chem. Eng. News* **2005**, *83*, 32−35.
(28) Siebert, H.; Weise, M. *Z. Naturforsch., B: Chem. Sci.* **1975**, *B30*, 33−39.
(29) Buser, H. J.; Ron, G.; Ludi, A. *J. Chem. Soc., Dalton Trans.* **1974**, 2473−2474.
(30) Ludi, A.; Guedel, H. U.; Ruegg, M. *Inorg. Chem.* **1970**, *9*, 2224−7.
(31) Herren, F.; Fischer, P.; Ludi, A.; Haelg, W. *Inorg. Chem.* **1980**, *19*, 956−9.
(32) Chupas, P. J.; Ciraolo, M. F.; Hanson, J. C.; Grey, C. P. *J. Am. Chem. Soc.* **2001**, *123*, 1694−1702.
(33) Beno, M. A.; Kurtz, C.; Munkholm, A.; Rutt, U.; Engbretson, M.; Jennings, G.; Linton, J.; Knapp, G. S.; Montano, P. A. *Nucl. Instrum. Methods Phys. Res., Sect. A* **2001**, *467*, 694−698.
(34) Rutt, U.; Beno, M. A.; Strempfer, J.; Jennings, G.; Kurtz, C.; Montano, P. A. *Nucl. Instrum. Methods Phys. Res., Sect. A* **2001**, *467*, 1026−1029.
(35) Chupas, P. J.; Qiu, X.; Hanson, J. C.; Lee, P. L.; Grey, C. P.; Billinge, S. J. L. *J. Appl. Crystallogr.* **2003**, *36*, 1342−1347.
(36) Hammersley, A. P. ESRF Internal Report, 1997, ESRF97HA02T.
(37) Hammersley, A. P.; Svensson, S. O.; Hanfland, M.; Fitch, A. N.; Häusermann, D. *High-Pressure Res.* **1996**, *14*, 235−248.
(38) Larson, A. C.; Dreele, R. B. V. General Structure Analysis System (GSAS), 2000, Los Alamos National Laboratory Report, LAUR 86-748.

to the data. Apparent discontinuities in the thermal expansion measured for some compounds accompanied occasional instability of the synchrotron beam, that is, the incident wavelength.[39] These discontinuities were not reproduced in duplicate measurements and are unrelated to the true thermal expansion. Where possible, experiments were repeated; however, for some compounds a reduced temperature range was used to determine the CTE.

For the cubic systems (M = Mn, Fe, Co, Ni, Zn, Cd), the bridging carbon and nitrogen atoms were refined with anisotropic atomic displacement parameters with the space group $Fm\bar{3}m$. The atomic displacement parameters for the metal centers were constrained by symmetry to be isotropic. At low temperatures, the atomic displacement parameters for some of the M atoms refined to small negative values. This is likely to be the combined result of an oblique incidence effect[40−42] and correlations between the background and atomic displacement parameters.[43] The temperature dependence of these parameters and the trends with composition, on which the ensuing analysis is focused, remains unperturbed by such effects. For the tetragonally distorted $CuPt(CN)_6$ phase, careful refinement of the structural parameters within the space group *I*4/*mmm* reproduced the peak position and approximate intensities (see Supporting Information). Slight deviations in the peak intensities, most notable at low angle and possibly arising from a subtle local ordering effect, prevented an unconstrained structural refinement. The subsequent analysis focuses on the structures refined for the cubic phases.

Raman Spectroscopy. Raman spectra were collected on samples of $M^{II}Pt^{IV}(CN)_6 \cdot 2\{H_2O\}$ (M = Mn, Fe, Co, Cu, Zn, Cd) in the range 80−3500 cm^{-1} using a Bruker FT-Raman spectrometer with an excitation wavelength of 1064 nm. The spectra of representative samples did not change visibly upon dehydration at high temperature with the exception of the absence of the broad peak at ca. 1500 cm^{-1} associated with the guest water molecules. All reported spectra and vibrational frequencies relate to data measured on as-prepared hydrated samples. It was not possible to measure the Raman spectrum for $NiPt(CN)_6$ due to decomposition of the sample in the beam. The spectra for M = Fe, Co, Cu contained large contributions to the background from sample fluorescence.

Results

Thermal Expansion Behavior. Approximately linear NTE behavior was evident for all Prussian Blue analogues $M^{II}Pt^{IV}(CN)_6$ for M = Mn, Fe, Co, Ni, Cu, Zn, Cd, over the temperature range measured (Figure 2).

The magnitude of the NTE behavior varies widely with M^{II} substitution (Table 1), from near zero thermal expansion in $NiPt(CN)_6$ ($\alpha = -1.02 \times 10^{-6}$ K^{-1}) up to a maximum in $CdPt(CN)_6$ ($\alpha = -10.02 \times 10^{-6}$ K^{-1}),[44] greater than the NTE behavior reported for ZrW_2O_8 ($\alpha = -9.1 \times 10^{-6}$ K^{-1}).[6] The degree of NTE behavior followed the order for M = Mn^{II} > Fe^{II} > Co^{II} > Ni^{II} < Cu^{II} < Zn^{II} < Cd^{II}, with the CTEs becoming progressively less negative and then more negative with increasing atomic number (*Z*) of the M^{II} ion (Figure 3). This follows the same trend as the lattice dimensions, which varies almost linearly with M^{II} cation size,[45] with more pronounced NTE behavior evident for analogues with larger lattices.

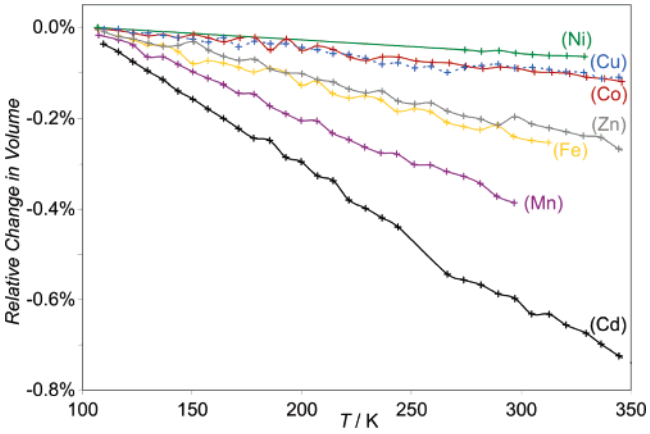

Figure 2. The temperature dependence of the unit cell volume relative to the volume at 100 K for $M^{II}Pt^{IV}(CN)_6$ (M = Mn, Fe, Co, Ni, Cu, Zn, Cd).

Table 1. Lattice Parameters (*a*) and Coefficients of Thermal Expansion (α) for $M^{II}Pt^{IV}(CN)_6$

compound	*a*(100 K)/Å	$\alpha/\times 10^{-6}$ K^{-1}	*T*/K
$MnPt(CN)_6$	10.8338	−6.58(9)	100−300
$FePt(CN)_6$	10.6615	−4.00(7)	100−315
$CoPt(CN)_6$	10.5665	−1.60(6)	100−350
$NiPt(CN)_6$	10.4680	−1.02(11)	100−330
$CuPt(CN)_6$[a]	$a = 7.3392$	$\alpha_a = -5.01(6)$	100−400
	$c = 11.0516$	$\alpha_c = +5.26(17)$	
$ZnPt(CN)_6$	10.6541	−3.53(5)	100−400
$CdPt(CN)_6$	11.0210	−10.02(11)	100−240

[a] Effective linear CTE ($\alpha_{volume}/3 = -1.57(7) \times 10^{-6}$ K^{-1}) for tetragonal $CuPt(CN)_6$.

While the thermal expansion behavior is isotropic (defined) for the cubic systems, highly anisotropic behavior was evident for the tetragonally distorted $CuPt(CN)_6$. The Jahn−Teller elongated Cu^{II} axis, which is aligned parallel to the crystallographic *c*-axis, expands upon heating. By contrast, the *a*-axis contracts upon heating. The absolute magnitude of the thermal expansion in each direction was greater than that of the immediately adjacent cubic analogues; however, the overall NTE behavior of the cell volume corresponds to an intermediate linear CTE ($\alpha_{volume}/3$).

Structural Refinement. The Rietveld refined structural models are consistent with the reported topology for $M^{II}Pt^{IV}$-

(39) The 11-ID-B beamline uses a single reflection Laue monochromator to select the incident wavelength on the elliptical multipole wiggler insertion device beamline (Sector 11) at the Advanced Photon Source at Argonne National Laboratory (refs 33 and 34). The elliptical multipole wiggler has a high critical energy and is thus capable of producing a large heat load on the beamline optics. Fluctuations in the temperature of the monochromator crystal arising from beam instabilities, including occasional interruptions to continuous fill (i.e., "top-up") operations, resulted in fluctuations in the reflected X-ray energy.

(40) Wu, G.; Rodrigues, B. L.; Coppens, P. *J. Appl. Crystallogr.* **2002**, *35*, 356−359.

(41) Zaleski, J.; Wu, G.; Coppens, P. *J. Appl. Crystallogr.* **1998**, *31*, 302−304.

(42) The present experimental configuration was associated with an oblique-incidence effect, which arises from incomplete absorption of the incident beam in the phosphor layer of the flat imaging plate, such that the path length of the diffracted beam in the phosphor (and the measured intensity) varied with angle of incidence (i.e., diffraction angle). Consequently, greater apparent relative peak intensities were measured at higher angles, an effect which artificially lowers the refined atomic displacement parameters. While a general correction for oblique incidence exists, it requires the phosphor absorption to be known at the X-ray energy used and does not consider the variable penetration depth of the image plate readout laser. As such, an accurate correction to the intensities is unavailable.

(43) The more significant peak overlap at high angles can lead to the underestimation of the background. The corresponding greater apparent peak intensities measured at higher angles can artificially bias the atomic displacement parameters to lower values.

(44) The CTE found here for $CdPt(CN)_6$ is noticeably more negative than that measured previously (ref 23). Initial $K_2Pt(CN)_6$ samples (Sigma-Aldrich) were pale yellow, yielding the pale yellow crystals of $CdPt(CN)_6$ used in the early single-crystal studies. Subsequent $K_2Pt(CN)_6$ samples were colorless, as is consistent with the compound description, yielding the colorless $CdPt(CN)_6$ sample used here. The earlier measurements are believed to be affected by the incorporation of the yellow contaminant from the $K_2Pt(CN)_6$ precursor into the single-crystal samples. All samples being compared here were prepared using a single sample of colorless $K_2Pt(CN)_6$ precursor.

(45) Shannon, R. *Acta Crystallogr., Sect. A* **1976**, *32*, 751−767.

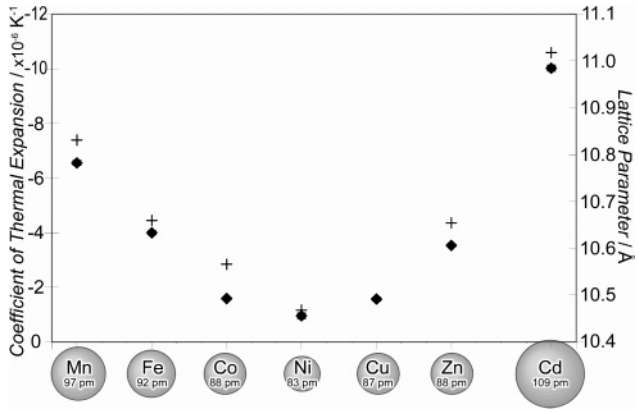

Figure 3. Linear coefficients of thermal expansion (◆) and cubic lattice parameters at 100 K (+) for $M^{II}Pt^{IV}(CN)_6$ (M = Mn, Fe, Co, Ni, Cu, Zn, Cd) in order of increasing Z of the M^{II} ion. The M^{II} ionic radii are indicated.[45]

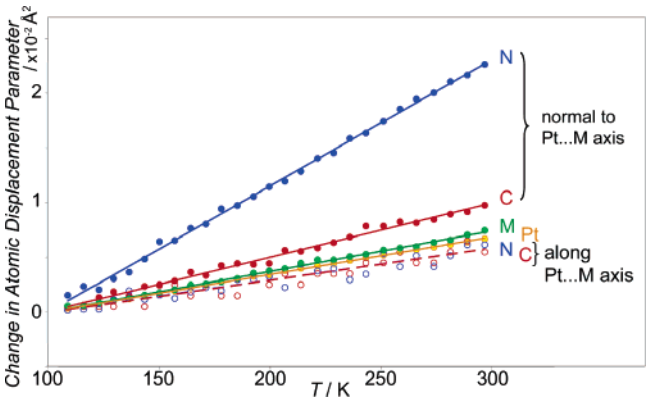

Figure 4. Increases in the atomic displacement parameters for $MnPt(CN)_6$ relative to the values at 100 K.

$(CN)_6$.[28,29,23] The high quality of the data obtained by integration of the scattered intensity over a complete solid angle, and the measurement of data to very short *d*-spacings enabled by high X-ray energies, allowed full anisotropic refinement of the structure with minimal correlations of the refinement parameters, including for the comparatively weakly scattering carbon and nitrogen atoms.

The temperature dependence of the Rietveld refined structure for each Prussian Blue analogue shows approximately linear increases in the atomic displacement parameters upon heating (Figure 4). For the bridging cyanide atoms, more rapid increases were observed for the components of the atomic displacement parameters perpendicular to the $M^{II}\cdots Pt^{IV}$ axis than for those along the $M^{II}\cdots Pt^{IV}$ axis. This observation is consistent with the thermal population of low-energy transverse vibrational modes of the cyanide bridges, which underlies the NTE behavior in this system. More rapid increases were observed for the atomic displacement parameters of the M^{II}-bound nitrogen atom than for the Pt^{IV}-bound carbon atom. The parallel components of the atomic displacement parameters for the bridging atoms typically had large errors, possibly containing a contribution from bonding electron density.

Within the series of Prussian blue analogues, the rates of change of the atomic displacement parameters with temperature ((dU/dT)'s) follow the same trend as for the magnitude of the NTE behavior, such that more rapid increases in the atomic displacement parameters occur in phases that have more pronounced NTE behavior. Most sensitive to M^{II} substitution was the perpendicular component of the nitrogen atomic displacement parameter, followed by the isotropic displacement parameter of the M atom and the perpendicular component of the carbon displacement parameter (Figure 5).

The $M^{II}-N$ and $Pt^{IV}-C$ bond lengths inferred from the Rietveld refined average structure for each Prussian Blue analogue showed a slight contraction or no significant change with heating. The apparent unphysical bond length contraction is typical of such NTE materials and arises from the deviation of the average (Rietveld refined) and instantaneous structures; such an effect is consistent with the transverse vibrational mechanism for NTE behavior.[17,46]

The $M^{II}-N$ bond lengths in the series of Prussian Blue analogues were in the range 2.08−2.21 Å and showed the greatest sensitivity to M^{II} substitution, with the bond length following the same trend as for the M^{II} cation size (Figure 6). The $Pt^{IV}-C$ bond lengths were in the range 2.00−2.21 Å and showed less systematic variation with M^{II} substitution.

Raman Spectroscopy. A representative Raman spectrum for $MnPt(CN)_6$ indicating peak assignments[47] is shown in Figure 7. The vibrational frequencies from spectra for $M^{II}Pt^{IV}(CN)_6$ are given in Table 2. The $CuPt(CN)_6$ spectrum has additional peaks relative to the spectra for cubic $M^{II}Pt^{IV}(CN)_6$ due to its lower symmetry.

The frequencies of the bending and stretching modes in the series $M^{II}Pt^{IV}(CN)_6$ for M = Mn, Fe, Co, Cu, Zn, Cd increase and then decrease with increasing Z of the M^{II} ion, following

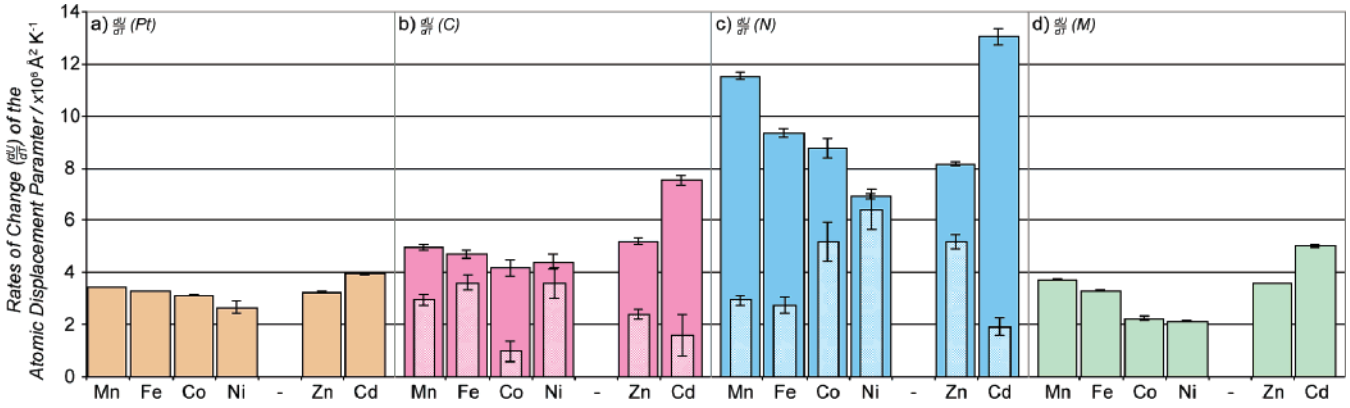

Figure 5. Temperature dependence of the atomic displacement parameters ((dU/dT)'s) from the least-squares linear fits to the data for (a) platinum, (b) carbon perpendicular and parallel (inner bars) to the $Pt^{IV}\cdots M^{II}$ axis, (c) nitrogen perpendicular and parallel (inner bars) to the $Pt^{IV}\cdots M^{II}$ axis, and (d) M^{II} for $M^{II}Pt^{IV}(CN)_6$ in order of increasing Z of the M^{II} ion. The errors are given as ±1 esd.

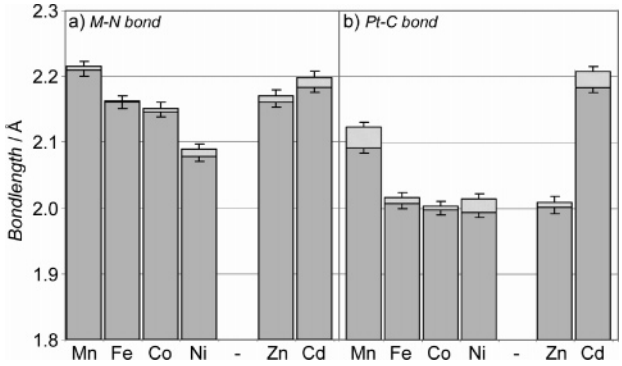

Figure 6. The (a) $M^{II}-N$ and (b) $Pt^{IV}-C$ bond lengths inferred from the Rietveld refined average structures of $M^{II}Pt^{IV}(CN)_6$ in order of increasing Z of the M^{II} ion. The ranges of the temperature-dependent bond lengths are indicated (shaded area).

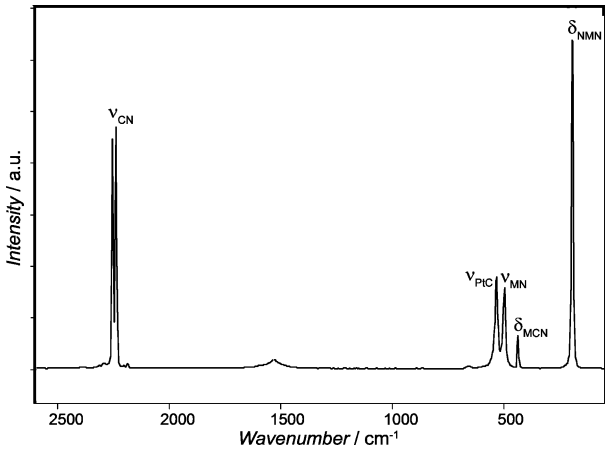

Figure 7. Raman spectrum for $MnPt(CN)_6$.

Table 2. Vibrational Frequencies for $M^{II}Pt^{IV}(CN)_6$ from Raman Spectroscopy

	ν(CN)/cm^{-1}	ν(PtC)/cm^{-1}	ν(MN)/cm^{-1}	δ(MCN)/cm^{-1}	δ(NMN)/cm^{-1}
$MnPt(CN)_6$	2236, 2251	533	496	435	192
$FePt(CN)_6$	2239, 2253	539	503	436	208
$CoPt(CN)_6$	2243, 2255	541	506	438	216
$CuPt(CN)_6$	2223, 2254, 2267	569	472, 504	432	194, 267
$ZnPt(CN)_6$	2243, 2260	549	493	438	219
$CdPt(CN)_6$	2236, 2251	534	491	431	176

the same trend as the magnitude of the NTE behavior in this series. Although the observed Raman peaks are of higher energy than the lowest energy peak reported in the inelastic neutron scattering spectrum for $ZnPt(CN)_6$ at 7.5 meV ($\sim$60 cm^{-1}),[48] the spectra provide an indication of the general compositional dependence of the framework flexibility. As such, enhanced NTE behavior is seen for the more flexible members of this series with lower frequency Raman modes.

Discussion

The magnitude of the NTE behavior in the $M^{II}Pt^{IV}(CN)_6$ series of Prussian Blue analogues follows the order for M = Mn^{II} > Fe^{II} > Co^{II} > Ni^{II} < Cu^{II} < Zn^{II} < Cd^{II}, which correlates with the trends both in the vibrational flexibility as indicated by the Raman spectroscopic studies and in the relative rates of increase with temperature of the atomic displacement parameters from Rietveld refinement. This observation is consistent with the transverse vibrational mechanism for the NTE behavior and the expectation that lower energy modes are populated more rapidly with heating. Consequently, more pronounced NTE behavior is associated with "floppier" frameworks, that is, those having lower energy vibrational modes, with these modes predominantly associated with lattice contraction, involving transverse vibrations of the cyanide bridge.

In the present series of Prussian Blue frameworks, the variation in the structural flexibility and, accordingly, the differences in the magnitude of the NTE behavior appear to arise principally from the difference in strength of the $M^{II}-NC$ binding interaction. This is evident experimentally from the greater variation with M^{II} substitution of the temperature dependence of the perpendicular displacement parameters for the M^{II}-bound nitrogen atom as compared to the Pt^{IV}-bound carbon atom, a parameter that includes a contribution from the transverse vibrational motion of the cyanide bridge. For high spin M^{II} ions, the strength of the $M^{II}-$ligand binding interaction follows the Irving–Williams series for metal complex stability, based on crystal field and ionic radii considerations, with the order Mn^{II} < Fe^{II} < Co^{II} < Ni^{II} > Cu^{II} > Zn^{II} > Cd^{II}. As expected, this follows a trend inverse to that of the magnitude of the observed NTE behavior, with the decreased structural flexibility associated with stronger $M^{II}-N$ bonds resulting in reduced NTE behavior. This underlies the correlation between the magnitude of the thermal expansion behavior and the M^{II} cation size.

Seemingly similar parallels between cation size and the magnitude of NTE behavior have been reported within some oxide-based series. However, in those cases, the correspondence can be attributed to a separate mechanism particular to the framework topology: in the AM_2O_7 and $A_2M_3O_{12}$ families,[9,11] the transverse vibrational motion underlying NTE behavior induces an energetically unfavorable distortion in the metal ion coordination, a dampening effect that is reduced for larger cations with more flexible coordination geometry. In the Prussian Blue topology, and those of many other NTE materials, it is possible for the transverse vibrational modes to be correlated such that the metal ion coordination geometry remains unchanged.[21,49,50] A correlation between the low-temperature lattice parameter and the NTE behavior has been noted for the family $ZrW_{2-x}Mo_xO_8$ (x = 0, 1, 2). There, different cooling rates affect ordering of the oxygen atoms, altering the low-temperature lattice parameter for a given sample and varying the thermal expansion behavior determined subsequently upon heating.[18] In the $CuMO_2$ (M^{III} = Al, Sc, In, La) series with the delafossite structure,[19] the complex thermal expansion behavior involves scissoring of Cu-linked $[MO_2]^-$ sheets coupled with a contraction along the O–Cu–O linkages induced by transverse Cu motion. The NTE behavior has been reported to increase as the size of M^{III} increases, with possible steric dampening of the transverse Cu modes due to shorter Cu···Cu contacts associated with smaller M^{III} ions/$[MO_2]^-$ sheets. This series of Prussian Blue analogues represent the first case where such an extensive series has been achieved, where the phases are truly isostructural

(46) Tucker, M. G.; Dove, M. T.; Keen, D. A. *J. Phys.: Condens. Matter* **2000**, *12*, L425–L430.
(47) Bowmaker, G. A.; Kennedy, B. J.; Reid, J. C. *Inorg. Chem.* **1998**, *37*, 3968–3974.
(48) Chapman, K. W.; Hagen, M. E.; Kepert, C. J.; Manuel, P. *Physica B*, in press.
(49) Heine, V.; Welche, P. R. L.; Dove, M. T. *J. Am. Ceram. Soc.* **1999**, *82*, 1793–1803.
(50) Pryde, A. K. A.; Hammonds, K. D.; Dove, M. T.; Heine, V.; Gale, J. D.; Warren, M. C. *J. Phys.: Condens. Matter* **1996**, *8*, 10973–10982.

and without phase transitions and where chemically relevant parameters beyond cation size can be correlated.

In the tetragonal $CuPt(CN)_6$ analogue, the alignment of the Jahn−Teller elongated axis of the Cu^{II} ion along the *c*-axis results in reduced symmetry and highly anisotropic thermal expansion behavior, with enhanced NTE behavior in the *ab*-plane and PTE behavior along the *c*-axis. It is interesting to note that the considerable weakening of the M^{II}−N bond through binding at the elongated Jahn−Teller axis actually results in PTE behavior along this direction, an effect contrary to the trend seen for weakening of the M^{II}−N bond with M^{II} substitution in the isotropic, cubic phases. This behavior indicates an expansion of the Cu···Pt distance along the *c*-axis with increasing temperature, which may be due to a greater contribution to the thermal expansion from the low-energy axial Cu^{II}−N stretching modes than from the low-energy transverse cyanide vibrations. The enhanced flexibility of the transverse cyanide modes along the *c*-direction is expected to decrease the energy of other, correlated modes; these notably include transverse vibrations of the cyanide linkages within the *ab*-plane, which are coupled to those along the *c*-direction through the Cu^{II} coordination sphere, a factor that may explain the enhanced NTE behavior in the *ab*-plane relative to that of the cubic Fe^{II}, Co^{II}, Ni^{II}, and Zn^{II} analogues. Hence, these observations are consistent with the expectation that the low-energy lattice modes in the Prussian Blue topology involve the correlation of the transverse vibrations such that the metal ion coordination geometry remains unchanged.[21]

The wide range of thermal expansion behaviors that can be accessed through M^{II} substitution in this series of Prussian Blue analogues is due, in part, to the fact that the transverse motion at the M^{II}-bound nitrogen atom has a greater contribution to the NTE behavior than the transverse motion at the carbon atom. This is evident in the less rapid increases with temperature in the perpendicular displacement parameters for the carbon atom and can be attributed to the correlation between bond strength and vibrational bending flexibility, with the more strongly binding tetravalent Pt^{IV} ions effectively dampening the transverse vibrations at the carbon atom. This underlies the less pronounced NTE behavior for the present series of cyanide-bridged molecular framework materials as compared to the $M(CN)_2$ family, with the CTE in $ZnPt(CN)_6$ being approximately one-fifth that observed for $Zn(CN)_2$.[17] The different flexibilities are reflected also in the phonon spectra for these phases, with low-energy bands for $Zn(CN)_2$ and $ZnPt(CN)_6$ observed at 2 and 7.5 meV, respectively.[48] Given the greater proposed influence on expansion properties of the local bending energy of the M^{II}−N−C unit as compared to that of Pt^{IV}−C−N, it is expected that metal substitution at the tetravalent site would have a lesser impact on the magnitude of the NTE behavior.

The magnitudes of NTE behavior spanned by this Prussian Blue series coincide with the magnitudes of PTE behavior for many common ceramic solids.[51] With the likely possibility of forming binary, or higher order, solid solutions of the type $M_xM'_{1-x}Pt(CN)_6$ (M, M′ = Mn, Fe...), it is anticipated that Prussian Blue analogues with CTEs varying continuously within the range -1×10^{-6} to -10×10^{-6} K^{-1} and customized toward particular applications may be achieved. This can be most directly envisaged in electronic and photonic applications where the thermal expansion behavior can be adjusted through composition alone without additional influence of guest sorption in the low moisture environment.[23] Moreover, the present $M^{II}Pt^{IV}(CN)_6$ series represents only a small subset of possible Prussian Blue analogues for which the rich compositional and structural diversity is expected to yield a vastly expanded range of NTE materials, possibly with enhanced NTE behavior or closer to zero thermal expansion behavior depending on the nature of the metal−cyanide interaction and structural topology.

Conclusion

Large differences are observed in the NTE behaviors in the series of Prussian Blue analogues $M^{II}Pt^{IV}(CN)_6$ for M = Mn, Fe, Co, Ni, Cu, Zn, Cd ($\alpha = -1.02(11) \times 10^{-6}$ to $-10.02(11) \times 10^{-6}$ K^{-1}). We propose that these differences are due principally to the varying strengths of the M^{II}−cyanide binding interaction and, accordingly, to the varying energies of transverse vibrational motion of the cyanide bridge. Such a mechanism is supported by systematic trends observed in the Rietveld refined structures and the Raman spectra for these phases. The distinctly anisotropic thermal expansion in the Jahn−Teller distorted Cu^{II} analogue, which has enhanced NTE behavior in the *ab*-plane and PTE behavior along the *c*-axis, supports the view that the transverse cyanide vibrations are strongly coupled through the metal coordination spheres. It is envisaged that the systematic structure−property relationships extracted from these results can be extended to understand NTE behavior in the broad family of Prussian Blue analogues (possibly the largest family of NTE materials), in other cyanide-bridged molecular frameworks, and in many oxide-based materials.

Acknowledgment. This work was supported by the Australian Research Council and the Australian Synchrotron Research Program, which is funded by the Commonwealth of Australia under the Major National Research Facilities. Work performed at the A.P.S. was supported by the U.S. D.o.E., Office of Science, Basic Energy Sciences, under Contract No. W-31-109-Eng-38. K.W.C. acknowledges a Joan R. Clark Research Scholarship. We thank M. E. Asplet, P. D. Southon, C. Kurtz, E. Carter, G. Jennings, and N. Leyarovska for experimental support.

Supporting Information Available: Details of the Rietveld analysis. This material is available free of charge via the Internet at http://pubs.acs.org.

JA060916R

(51) Taylor, D. *Br. Ceram. Trans. J.* **1984**, *83*, 5−9.